ChemComm

COMMUNICATION

View Article Online
View Journal | View Issue

Reversible stimulus-responsive Cu(I) iodide pyridine coordination polymer†

P. Amo-Ochoa,*[a] K. Hassanein,[a] C. J. Gómez-García,[b] S. Benmansour,[b] J. Perles,[c] O. Castillo,[d] J. I. Martínez,[e] P . Ocón[f] and F. Zamora*[ag]

Cite this: *Chem. Commun.*, 2015, 51, 14306

Received 9th June 2015,
Accepted 30th July 2015

DOI: 10.1039/c5cc04746c

www.rsc.org/chemcomm

We present a structurally flexible copper–iodide–pyridine-based coordination polymer showing drastic variations in its electrical conductivity driven by temperature and sorption of acetic acid molecules. The dramatic effect on the electrical conductivity enables the fabrication of a simple and robust device for gas detection. X-ray diffraction studies and DFT calculations allow the rationalisation of these observations.

In recent years, coordination polymers (CPs) have gained increasing attention due to their wide structural variety and interesting physico-chemical properties.[1] They are a potential source of multifunctional materials that can bring remarkable physical properties such as luminescence,[2] non-linear optics,[3] magnetism[4] and electrical conductivity.[5] CPs have the ability to produce dynamic structures due to the structural flexibility of the ligands and/or the ability of the coordination sites to exchange, release and/or re-accommodate molecules, rendering CPs as a source of stimuli-responsive materials.[6] These dynamic materials show potential applications as chemical switches, memories or molecular sensors.

A limited number of CPs have shown spin-crossover transitions modulated or induced by a chemical stimulus such as gas or solvent sorption in the pores[7–11] and magnetic, physically-driven solid-state transformation.[12,13] Stimuli-responsive electrical materials, mainly centred on organic conductive polymers,[14] are currently of high interest. A recent example of a thin-film device based on the porous coordination polymer $Cu_3(BTC)_2$ (BTC = benzene-1,3,5-tricarboxylic acid) has shown an electrical response to 7,7,8,8-tetracyanoquinodimethane (TCNQ) guest molecules.[15] Quasi-linear physical properties have also been reported for MX and MMX chains (M = transition metal, X = halide), some of them showing thermal Peierls transitions that affect their magnetic properties[16] and/or their electrical conductivity.[17]

Additionally, we have reported that some double-stranded Cu-halide stairs present interesting physical properties.[18] Here we disclose two 1D-CP polymorphs of Cu(I) with iodide as bridging ligands and 2-amino-5-nitropyridine ($C_5H_5N_3O_2$, ANP) as terminal ligands. These polymorphs show very flexible structures that enable a reversible physically-driven electrical conductive transition with electrical bi-stability close to room temperature and a chemically-driven transition that induces a dramatic enhancement of the electrical conductivity, allowing the fabrication of a simple and robust gas-detection device.

The direct reactions carried out between CuI and ANP at 25 °C or under solvothermal conditions lead to the isolation of $[Cu(C_5H_5N_3O_2)I]_n$ (**1**) and its polymorph **1a**, respectively. **1a** is isostructural to the Br derivative, also prepared under solvothermal conditions.[19] Both polymorphs show a double-stranded stair motif in which the Cu(I) centres are bridged by μ_3-I. Since the electrical properties (see below) of compound **1** indicate a phase transition at *ca.* 267–282 K, we have studied in detail the thermal dependence of the unit cell parameters of **1** (Fig. S1–S6, ESI†) and solved the structure of **1** at 200 K ($\mathbf{1^{LT}}$) and at 298 K ($\mathbf{1^{RT}}$). $\mathbf{1^{RT}}$, $\mathbf{1^{LT}}$ and **1a** contain Cu(I) ions with a tetrahedral environment formed by three bridging iodine ions and the iminic nitrogen atom of the 2-amino-5-nitropyridine ligand (Fig. 1).

The Cu–I and Cu–N bond distances are similar to those found in similar $[CuI(L)_n]$ stairs.[20–26] The intra-chain Cu···Cu

[a] *Departamento de Química Inorgánica, Universidad Autónoma de Madrid, 28049 Madrid, Spain. E-mail: felix.zamora@uam.es*
[b] *Instituto de Ciencia Molecular (ICMol), Parque Científico, Universidad de Valencia, Catedrático José Beltrán, 2. 46980 Paterna Valencia, Spain*
[c] *Servicio Interdepartamental de Investigación, Universidad Autónoma de Madrid, 28049 Madrid, Spain*
[d] *Departamento de Química Inorgánica, Universidad del País Vasco, Apartado 644, e-48080 Bilbao, Spain*
[e] *Instituto de Ciencia de Materiales CSIC, 28049 Madrid, Spain*
[f] *Departamento de Química Física Aplicada, Universidad Autónoma de Madrid, Madrid, Spain*
[g] *Condensed Matter Physics Center (IFIMAC), Universidad Autónoma de Madrid, 28049 Madrid, Spain*

† Electronic supplementary information (ESI) available: Experimental details, crystallographic data and structure refinement details of all the compounds, additional data of X-ray studies on thermal variation parameters of compound **1**, supramolecular interactions details and DFT calculations of $\mathbf{1^{LT}}$, $\mathbf{1^{RT}}$ and **1a**, and additional data of the studies on the device characterization based on compound **1**. CCDC 1046598–1046600. For ESI and crystallographic data in CIF or other electronic format see DOI: 10.1039/c5cc04746c

Published on 31 July 2015.

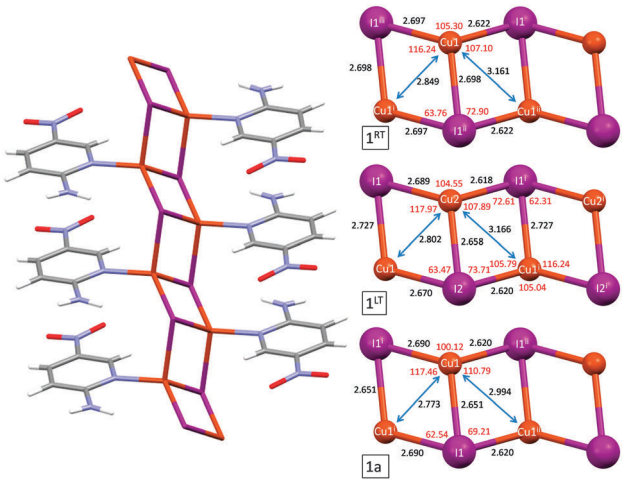

Fig. 1 (Left) View of the polymeric $[Cu(C_5H_5N_3O_2)I]_n$ chain in compounds **1** and **1a**. Colour code: orange (Cu), purple (I), grey (C), blue (N), red (O). (Right) Fragment of the double-stranded stair in $\mathbf{1}^{RT}$, $\mathbf{1}^{LT}$ and **1a** showing the bond angles (°) and distances (Å).

Table 1 D.C. conductivity values at 300 K and experimental and calculated activation energies of compounds $\mathbf{1}^{LT}$, $\mathbf{1}^{RT}$ and **1a**

Compound	σ_{300K} (S cm^{-1})	E_g (eV) exp.	E_g (eV) calc.
$\mathbf{1}^{LT}$	—	0.08	0.18
$\mathbf{1}^{RT}$	1.1×10^{-8}	0.40	0.59
1a	5.0×10^{-6}	0.37	0.31

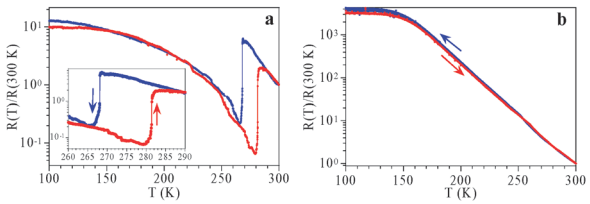

Fig. 2 Thermal variation of the normalized resistance of compounds **1** (a) and **1a** (b) in two successive cooling and heating and scans (1 and 2, respectively) in the 100–300 K range. Inset in (a) shows the reversible transition taking place at 268–281 K. The saturation of the resistance at low temperatures in both compounds indicates that the resistance has reached the limit of our equipment (5×10^{11} Ω).

Published on 31 July 2015.

distances are close to or below the sum of the van der Waals radii (2.80 Å). Interestingly, the Cu–I chain structure presents slight variations along the propagation direction (*a*), as shown by the unit cell *a* parameter (4.2284(1), 4.1982(1), and 4.0708(1) Å for $\mathbf{1}^{RT}$, $\mathbf{1}^{LT}$ and **1a**, respectively) and also reflected in the corresponding Cu–I–Cu and I–Cu–I bond angles along the chain (105.3° for $\mathbf{1}^{RT}$, 104.5–105.0° for $\mathbf{1}^{LT}$ and 100.1° for **1a**) (Fig. 1). Finally, the dihedral angle between adjacent Cu_2I_2 units along the chain also shows slight variations between both polymorphs (117.4° for $\mathbf{1}^{RT}$, 117.3° and 116.8° for $\mathbf{1}^{LT}$ and 114.1° for **1a**). These differences observed mainly between polymorphs **1** and **1a** suggest that the inter-chain interactions are important in determining the overall structures of these compounds, supporting the idea that the ANP ligand plays a crucial structural role. The ANP ring is tilted (78.2° for $\mathbf{1}^{RT}$, 79.0° for $\mathbf{1}^{LT}$ and 77.6° for **1a**) and twisted (57.4° for $\mathbf{1}^{RT}$, 56.0° for $\mathbf{1}^{LT}$ and 67.1° for **1a**) relative to the propagation direction of the chain. The chain cohesion is also ensured by the presence of π–π stacking interactions at both sides of the chain between adjacent ANP ligands with interplanar distances of 3.332 Å ($\mathbf{1}^{RT}$), 3.296 and 3.307 Å ($\mathbf{1}^{LT}$) and 3.520 Å (**1a**). All compounds show weak intra-chain hydrogen bonds involving the halide as acceptor and the NH_2/CH groups as donors thanks to the twisting of the ANP ligands. The nitro substituent of the ANP ligand plays a key role in assembling the chains together through hydrogen bonds between the NH_2 and C–H donor groups of neighbouring chains and the NO_2 group as an acceptor. Although similar interactions are present in these compounds, the total number of hydrogen bonds involving the ANP ligands differs (Fig. S7, ESI†). The order of hydrogen bond connectivity is $\mathbf{1}^{RT} < \mathbf{1}^{LT} <$ **1a**. Interestingly, the average intra-chain Cu···Cu distances are shorter in the dimerised phase ($\mathbf{1}^{LT}$) than in the regular one ($\mathbf{1}^{RT}$) (Fig. 1). **1a** shows shorter intra-chain Cu···Cu distances compared to $\mathbf{1}^{LT}$ and $\mathbf{1}^{RT}$.

Electrical conductivity measurements were carried out at 300 K (Table 1) show that the room-temperature average DC conductivity values are strongly dependent on the structure, with $\sigma(\mathbf{1a}) > \sigma(\mathbf{1})$, suggesting that the main factors determining the conductivity must be the structural parameters in the chain as the average Cu···Cu distance (3.01 Å in $\mathbf{1}^{RT}$, 2.98 Å in $\mathbf{1}^{LT}$ and 2.88 Å in **1a**) and the dihedral angle between adjacent Cu_2I_2 units, which is closer to 90° in **1a** (114.1°) than in $\mathbf{1}^{RT}$ (116.8–117.4°), resulting in a better orbital overlap in **1a**. Compound **1** presents a reversible semiconducting–semiconducting transition with an abrupt transition at *ca.* 267 K in the cooling scan and *ca.* 282 K in the heating scan along with a hysteresis of *ca.* 15 K (Fig. 2a). Interestingly, this transition implies a decrease in the resistivity by a factor of *ca.* 30 when passing from high to low temperature. Although the sample remains semiconducting before and after the transition, the activation energy decreases from *ca.* 0.40 eV at high temperatures to *ca.* 0.08 eV at low temperatures. These values indicate that the low temperature phase is a better conductor and has a lower activation energy, which is contrary to the usual behaviour observed in chain compounds, in which the Peierls transitions imply a decrease in resistivity and an increase in the energy gap in the low-temperature phase.[27–31] This unexpected result can be explained by the structural data obtained for $\mathbf{1}^{RT}$ and $\mathbf{1}^{LT}$ above and below the transition temperature. The main difference between $\mathbf{1}^{RT}$ and $\mathbf{1}^{LT}$ is the presence of two independent Cu and I atoms in $\mathbf{1}^{LT}$, compared to only one in $\mathbf{1}^{RT}$ and **1a**, resulting in a dimerised chain in $\mathbf{1}^{LT}$.

$\mathbf{1}^{LT}$ presents a more homogeneous distribution of the Cu–I bond distances, a shorter average Cu···Cu distance along the chain (Fig. 1) and a smaller dihedral angle between Cu_2I_2 units, suggesting that this phase must be a better conductor, in agreement with the experimental results. **1** and **1a** show very similar behaviours except for the transition at *ca.* 267–282 K that is only observed in **1** (Fig. 2b). Thus, **1a** shows an activation energy of 0.37 eV, but no transition (Fig. 2b).

Theoretical calculations show that the electronic structures yield minimum transport gap values at *Γ* points ranging from

0.18 to 0.59 eV for all the CPs (Fig. S8, ESI†), in excellent agreement with the experimental data (Table 1). These calculations[32] also show that **1** behaves as a typical p-type semiconductor with the Fermi level very close to the valence band. The valence and conduction band orbital electron isodensities for $\mathbf{1}^{RT}$, $\mathbf{1}^{LT}$ and **1a** (Fig. S9, ESI†) indicate a continuous hybridization band mostly located along the Cu–I skeleton and a continuous orbital side-to-side hybridization formed between the ligands, indicating that conduction takes place only along the chains. Increasing temperature allows charge migration from the valence band towards the conduction one along with a temperature-induced overlap between both bands, increasing the carrier mobility and the electronic conduction along the chains.

The flexible structure of **1** and the presence of ligands with available donor and acceptor H-bond groups prompted us to study the influence of external chemical stimuli in this material. Thus, when a microcrystalline powder of **1** is immersed in glacial acetic acid, a sorption process takes place, and the crystals change from yellow to orange and lose crystallinity, becoming amorphous (Fig. S10, ESI†). Surprisingly, this change is reversible; when the acetic acid is removed, and the sample is dried in air for several days, the crystals become yellow and recover their crystallinity (Fig. S10, ESI†).

This reversible interaction was also demonstrated by the change in the electrical conductivity of **1**. Thus, electrochemical impedance spectroscopy (EIS) measurements (Fig. 3) on a device built with a pellet of **1** electrically contacted with two copper wires (Fig. S11, ESI†) indicated a drastic reversible change in the conductivity when **1** was exposed to HAcO vapour for different exposure times. The Nyquist plot for compound **1** after 24 h of exposure to HAcO vapour in the frequency range of 1 Hz–1 MHz (Fig. 3a) shows the presence of a depressed semicircular arc at high-medium frequencies (1 MHz–30 Hz), which is attributed to the bulk properties of the compound, and a line in the low-frequency region, which is typical of materials with capacitive behaviour between the mobile ions (that are blocked by the electrode–electrolyte interphase).[33] The Nyquist plots recorded after different exposure times (45, 20 and 15 min) are similar to those obtained after 24 h of exposure (Fig. S12, ESI†); however, the intercept of the semicircle with the Z' axis shifts towards higher values. The plot of pristine sample **1** (t = 0 min in HAcO vapour) loses the semicircle shape. In addition, measurements from 100 Hz show high dispersion (Fig. S12, ESI†), suggesting that the material does not possess any inherent route for electrical conduction. The conductivity increases with increasing time of exposure to acetic acid vapour (Table S2, ESI†) and reaches saturation after *ca.* 45 minutes of exposure. In agreement with the Bode diagram, the semicircle representing the bulk properties of compound **1** is shifted to higher frequencies when the HAcO exposure time increases. This fact indicates that the material/electrode interphase capacitive character becomes less important, and the highly conductive phase of **1** appears (Fig. S12, ESI†). When saturated acetic acid pellets were exposed to air (30 min or longer times), the Nyquist plot lost the depressed semicircle shape, and a poor value of conductivity was obtained (*ca.* 10^{-11} S cm^{-1}). If we compare those results with the experiments involving different exposure times to HAcO vapour, the behaviour clearly indicates the crucial role of the HAcO molecules in establishing the conductivity pathway. The geometric capacitance values obtained in the high-medium frequency region (1 MHz–30 Hz) are *ca.* 10^{-11} F and are independent of the HAcO exposure time. However, the low-frequency tail, which could be assigned to the effect of electrode–electrolyte interactions and electrode polarization, gives capacitance values of 10^{-8}–10^{-6} F. However, this value is dependent on the composition and hence can be attributed to interfacial phenomena. In order to check the reversibility and cycling capacity of the observed drastic change in conductivity, after 12 h in air, the sample was re-exposed to HAcO vapour for 3 h. The Nyquist plot and the conductivity value (*ca.* 10^{-6} S cm^{-1}) were similar to the initial ones, confirming the total reversibility of the HAcO capture/release process and its effect on the conductivity of **1**. Successive on/off cycles (10 min in HAcO vapour followed by 70 min in air) yielded reproducible results (Fig. 4), confirming the stability of the device. Furthermore, we have verified that after several weeks in air, the device still exhibits the reproducible on/off cycles.

In a separate experiment, a pellet of **1** was exposed to CH_3Cl vapour for 24 h at 298 K (Table S2, ESI†). The EIS study at 298 K shows a conductivity of *ca.* 10^{-10} S cm^{-1}, indicating the weak influence of chloroform vapour compared to HAcO vapour. This result agrees with the idea that CH_3Cl presents a much lower capacity to interact with the ANP ligands in **1** (it has no H-bonding capacity) and, accordingly, has a negligible ability to modify the structural parameters of the CuI chain. In contrast,

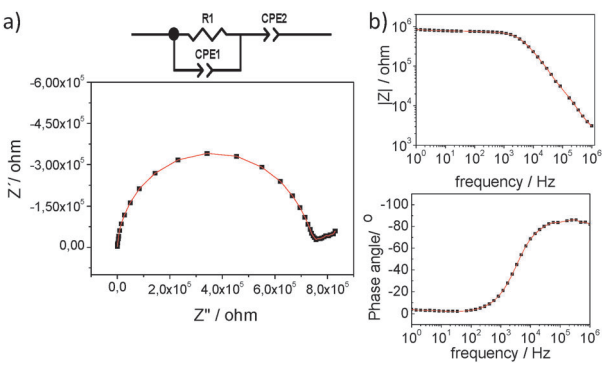

Fig. 3 Nyquist plot and equivalent circuit (a) and Bode plot (b) of compound **1** after 24 h of exposure to HAcO vapour: experimental values (■), fitting values (–).

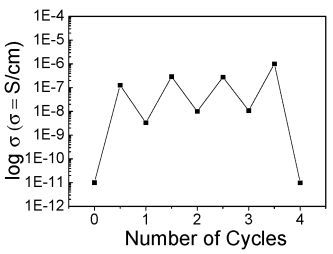

Fig. 4 Variation in conductivity during four on–off cycles of compound **1** at 298 K.

HAcO has a high H-bonding capacity and, accordingly, is expected to interact with the amino group of the ANP ligand and modify the structural parameters of the CuI chain, resulting in a drastic change in the conductivity.

Finally, in order to check if the absorbed acetic acid molecules induce any relevant structural changes in **1**, we have performed a powder X-ray diffraction study with a polycrystalline sample of **1** that was exposed to HAcO vapour for 24, 48 and 72 h. As expected, no dramatic structural changes in **1** were observed upon HAcO absorption (the powder X-ray diffractograms remain unchanged, Fig. S13 and S14, ESI†). This fact suggests that only a fraction of the sample becomes amorphous. Note that the capacity of HAcO molecules to interact with the ANP ligand and slightly modify the CuI chain cannot be ruled out.

CuI double chain compounds with ANP as terminal ligand are very sensitive to external physical and chemical stimuli. We have prepared two polymorphs (**1** and **1a**) of $[Cu(C_5H_5N_3O_2)I]_n$, allowing a detailed study of the effects of the structural parameters of the CuI chain on the electrical properties. Polymorph **1** shows a reversible thermally-induced transition with a hysteresis of *ca.* 15 K near room temperature, implying an unprecedented increase in conductivity (*ca.* 30-fold) in the low-temperature phase. This transition is due to slight reversible variations in the Cu/I bond distances and angles. The theoretical calculations suggest that the conduction mechanism seems to be produced exclusively along the one-dimensional chains. Furthermore, the extraordinary capacity of these chains to respond to chemical stimuli is exemplified by the behaviour observed in a device prepared with **1** that shows a reversible increase/decrease in conductivity of *ca.* 4 orders of magnitude due to the uptake/release of HOAc in the structure. The high capacity of **1** to respond to external stimuli is attributed to two facts: (i) the softness of the double CuI chains that makes these chains very dynamic and easy to distort, leading to huge changes in electrical conductivity; and (ii) the presence of ANP as terminal ligand directly connected to the CuI chains, acting as an antenna for the external chemical stimuli.

We are thankful for support from MICINN (MAT2013-46753-C2-1-P, MAT2013-46502-C2-1/2-P and CTQ2011-26507), Eusko Jaurlaritza (S-PE13UN016) and Generalitat Valenciana (PrometeoII/2014/076). J.I.M. thanks CSIC-JAEDOC.

Notes and references

1 S. R. Batten, S. M. Neville and D. Turner, *Coordination Polymers: Design, Analysis and Applications*, RSC Pub., 2009.
2 Y. J. Cui, Y. F. Yue, G. D. Qian and B. L. Chen, *Chem. Rev.*, 2012, **112**, 1126–1162.
3 C. Wang, T. Zhang and W. B. Lin, *Chem. Rev.*, 2012, **112**, 1084–1104.
4 M. Kurmoo, *Chem. Soc. Rev.*, 2009, **38**, 1353–1379.
5 G. Givaja, P. Amo-Ochoa, C. J. Gomez-Garcia and F. Zamora, *Chem. Soc. Rev.*, 2012, **41**, 115–147.
6 See the recent themed issues on MOFs: (*a*) *Chem. Soc. Rev.*, 2009, 1201–1508; (*b*) *Chem. Rev.*, 2012, **112**, 673–1268.
7 M. C. Munoz and J. A. Real, *Coord. Chem. Rev.*, 2011, **255**, 2068–2093.
8 J. Ferrando-Soria, P. Serra-Crespo, M. de Lange, J. Gascon, F. Kapteijn, M. Julve, J. Cano, F. Lloret, J. Pasan, C. Ruiz-Perez, Y. Journaux and E. Pardo, *J. Am. Chem. Soc.*, 2012, **134**, 15301–15304.
9 E. Coronado, M. Gimenez-Marques, G. M. Espallargas and L. Brammer, *Nat. Commun.*, 2012, **3**, Artn 828.
10 J. S. Costa, S. Rodriguez-Jimenez, G. A. Craig, B. Barth, C. M. Beavers, S. J. Teat and G. Aromi, *J. Am. Chem. Soc.*, 2014, **136**, 3869–3874.
11 E. Coronado, M. Gimenez-Marques, G. M. Espallargas, F. Rey and I. J. Vitorica-Yrezabal, *J. Am. Chem. Soc.*, 2013, **135**, 15986–15989.
12 E. Coronado, M. C. Gimenez-Lopez, G. Levchenko, F. M. Romero, V. Garcia-Baonza, A. Milner and M. Paz-Pasternak, *J. Am. Chem. Soc.*, 2005, **127**, 4580–4581.
13 E. Coronado, M. C. Gimenez-Lopez, T. Korzeniak, G. Levchenko, F. M. Romero, A. Segura, V. Garcia-Baonza, J. C. Cezar, F. M. F. de Groot, A. Milner and M. Paz-Pasternak, *J. Am. Chem. Soc.*, 2008, **130**, 15519–15532.
14 R. Yerushalmi, A. Scherz, M. E. van der Boom and H. B. Kraatz, *J. Mater. Chem.*, 2005, **15**, 4480–4487.
15 A. A. Talin, A. Centrone, A. C. Ford, M. E. Foster, V. Stavila, P. Haney, R. A. Kinney, V. Szalai, F. El Gabaly, H. P. Yoon, F. Leonard and M. D. Allendorf, *Science*, 2014, **343**, 66–69.
16 W. Fujita, K. Awaga, R. Kondo and S. Kagoshima, *J. Am. Chem. Soc.*, 2006, **128**, 6016–6017.
17 M. Yamashita and H. E. Okamoto, *Material Designs and New Physical Properties in MX- and MMX-Chain Compounds*, Springer-Verlag Wien, 2013.
18 E. Mateo-Marti, L. Welte, P. Amo-Ochoa, P. J. S. Miguel, J. Gomez-Herrero, J. A. Martin-Gago and F. Zamora, *Chem. Commun.*, 2008, 945–947.
19 W.-W. Zhou, W. Zhao, X. Zhao, F.-W. Wang and B. Wei, *Synth. React. Inorg., Met.-Org., Nano-Met. Chem.*, 2013, **43**, 1171–1174.
20 E. Cariati, D. Roberto, R. Ugo, P. C. Ford, S. Galli and A. Sironi, *Inorg. Chem.*, 2005, **44**, 4077–4085.
21 E. Cariati, D. Roberto, R. Ugo, P. C. Ford, S. Galli and A. Sironi, *Chem. Mater.*, 2002, **14**, 5116–5123.
22 F. Thébault, S. A. Barnett, A. J. Blake, C. Wilson, N. R. Champness and M. Schröder, *Inorg. Chem.*, 2006, **45**, 6179–6187.
23 T. H. Kim, Y. W. Shin, J. S. Kim, S. S. Lee and J. Kim, *Inorg. Chem. Commun.*, 2007, **10**, 717–719.
24 S.-M. Fang, Q. Zhang, M. Hu, B. Xiao, L.-M. Zhou, G.-H. Sun, L.-J. Gao, M. Du and C.-S. Liu, *CrystEngComm*, 2010, **12**, 2203–2212.
25 R.-F. Song, Y.-B. Xie, J.-R. Li and X.-H. Bu, *CrystEngComm*, 2005, **7**, 249–254.
26 Y. Takemura, T. Nakajima and T. Tanase, *Dalton Trans.*, 2009, 10231–10243.
27 J. Bernasconi, P. Büesch, D. Kuse and H. R. Zeller, *J. Phys. Chem. Solids*, 1974, **35**, 145–157.
28 L. B. Coleman, M. J. Cohen, D. J. Sandman, F. G. Yamagishi, A. F. Garito and A. J. Heeger, *Solid State Commun.*, 1973, **12**, 1125–1132.
29 J. Ferraris, D. O. Cowan, V. Walatka and J. H. Perlstein, *J. Am. Chem. Soc.*, 1973, **95**, 948–949.
30 F. Wudl, G. M. Smith and E. J. Hufnagel, *J. Chem. Soc. D*, 1970, 1453–1454.
31 R. E. Peierls, *Quantum Theory of Solids*, Oxford University Press, Oxford, 1955.
32 J. Troyano, J. Perles, P. Amo-Ochoa, J. I. Martinez, F. Zamora and S. Delgado, *CrystEngComm*, 2014, **16**, 8224–8231.
33 R. A. Huggins, *Ionics*, 2002, **8**, 300–313.